Advanced Steel Construction – Vol. 15 No. 3 (2019) 242–251
DOI:10.18057/IJASC.2019.15.3.4

RESISTANCE OF COLD-FORMED HIGH STRENGTH STEEL ANGLES

Anh Tuan Tran [1, *], Lars Bernspång [1], Milan Veljkovic [2], Carlos Rebelo[3] and Luís Simões da Silva [3]

[1] *Luleå University of Technology, Sweden*
[2] *Delft University of Technology, The Netherlands*
[3] *ISISE, University of Coimbra, Portugal*
** (Corresponding author: E-mail: trananhtuangtvt@gmail.com)*

ABSTRACT

This paper describes a study of the behaviour of cold-formed high strength steel angles. Thirty-six specimens with different cold-formed angles (90°, 100°, 120°, 140°, 160°, and 170°) and different thicknesses (4 mm and 6 mm) were considered. The initial geometric imperfections of the specimens were determined using the 3D laser scanning method. The magnitudes of these geometric imperfections for torsional and torsional-flexural buckling and flexural buckling analyses were proposed. The commercial finite element analysis (FEA) programme ABAQUS with shell elements S4R was used for finite element analyses. Different material strengths in corner and flat parts along with different proof stresses (0.2%, 0.01%, and 0.006%) were considered in the numerical models. The experimental and FEA results showed good agreement. Influence of cold-formed angle on non-dimensional slenderness and reduction factor curves of the 4 mm thick columns with 90° and 120° cold-formed angles was analysed.

ARTICLE HISTORY

Received: 19 March 2018
Revised: 20 December 2018
Accepted: 28 December 2018

KEYWORDS

High strength steel;
Cold-formed angle;
Geometrical imperfections;
Proof stress;
Experimental investigation;
Finite element analysis;

1. Introduction

The use of high strength steel material for cold-formed members significantly improves their properties. It enables thinner, longer and stronger structures. Moreover, the quantity of steel material required for building cold-formed steel structures is considerably reduced, and producing a beneficial effect on the environment. There are several standards that can be used for designing cold-formed steel structures: Australian/New Zealand cold-formed steel structures standard (AS/NZS-4600) [1], North American Specification for the design of cold-formed steel structural members (AISI-S100-12) [2] and European standard EN 1993-1-3 [3].

Several studies about cold-formed angles have been published [4 – 11]. Cold-formed steel angles are considered as thin-walled members that are sensitive to effects of imperfections. The imperfections including initial geometric imperfects and loading eccentricity significantly reduce their buckling strength. However, it is hardly to eliminate the imperfections because of manufacturing tolerance, transportation and measurement. Popovic et al. (1999) experimentally studied 12 fixed-ended and 18 pin-ended cold-formed angles under axial compression load [4]. The thicknesses used were 2.5 mm, 4 mm and 5 mm. As well as material investigations using tensile coupon tests, residual strains were measured with a Cambridge Insitu Extensometer and initial geometric imperfections were determined using a theodolite. The authors of that paper reported that experimental results were between 15% and 40% higher than the Australian and American specifications, respectively and additional eccentricity of L/1000 should only be applied to slender sections. It notes that nominal eccentricity of L/1000 about the minor axis was used for 18 pin end tests. Young (2004) carried out 24 compression tests on fixed-ended cold-formed plain angle columns [5]. The angles were produced using the press brake method. The thicknesses of the columns were 1.2 mm, 1.5 mm and 1.9 mm. The materials used were high strength zinc-coated steel grades G500 and G450. The experimental results were compared with American and Australian/New Zealand standards, and design rules for such fixed-ended cold-formed plain angle columns under compression load were proposed. He noted that additional moment (axial load multiplied by an eccentricity of L/1000) is used in design of compression members according to the AISI Specification and AS/NZS Standard. Ellobody et al. (2005) numerically investigated the behaviour of cold-formed steel plain angle columns [6]. Shell elements S4R in ABAQUS software were used for these investigations, which took into account initial geometric imperfection, residual stresses and material nonlinearities. Experimental and FEA results for 21 columns showed good agreement. The numerical models were developed for a parametric study, the results of which generally fitted design strengths calculated using equations described by Young [5]. Yang et al. (2011) studied buckling behaviour of cold-formed angles in transmission tower applications [7]. One series of equal angle specimens and three series of equal lipped angle specimens were considered. The angle specimens with different slenderness ratios and six constrained types were studied under axial compression load. The slenderness ratios were calculated based on minimum radius of gyration and length of specimens. The six constrained types at the end of the specimens were considered to reflect conditions of compression members in transmission towers. The six constrained types were determined based on slenderness ratio of the specimen and number of bolts used for the constraint. Shell elements SHELL181 in ANSYS software were used for a numerical investigation. FEA results were compared to experimental results, with the relationship between slenderness ratios and stability coefficients being modelled with a fitting curve and modification factors. Silvestre et al. (2013) summarised the development of the design of cold-formed steel angles [8]. The designs of fixed-ended and pin-ended equal-leg angle columns with short-to-intermediate lengths were considered. The experimental and FEA results from previous studies were taken into account in the study. The authors also described new design procedures based on the direct strength method (DSM). Shifferaw et al. (2014) presented a study of cold-formed steel lipped and plain angle columns with fixed ends [9]. In this study, the authors used ABAQUS with shell elements S9R5 to carry out a numerical investigation. Numerical models for fixed-ended and pin-ended angles with fixed and free warping were considered, with elastic critical buckling loads from the numerical investigations being compared to Young's experimental results. The authors presented new design procedures for strength prediction of the cold-formed angle columns. Resistance of cold-formed L columns under compression, bending and combination of compression and bending were investigated and reported in [10]. The L columns with different cold-formed angles and different thicknesses and with fixed and pinned boundary conditions were considered. Steel materials S650 and S500 were used in the study. As tensile coupon tests had not been carried out, the authors carried out FEA based on basic material properties. Influence of cold forming in hand calculation was considered according to EN 1993-1-3[3] based on nominal yield strength of the materials. Parametric study and comparison analyses were carried out. The authors recommend some changes in design procedure for cross sections with fixed boundary conditions. Landesmann et al. (2017) investigated the behaviour of short-to-intermediate slender pin-ended cold-formed steel equal-leg angle columns [11]. Nineteen columns with 1.55 mm nominal thickness, different leg widths (50 mm, 60 mm, 70 mm, 80 mm and 90 mm) and lengths ranging from 500 mm to 1200 mm were considered. The specimens were made of ZAR-345 mild steel. ANSYS software with shell elements SHELL181 was used for numerical investigation. Amplitude L/1000 was used for numerical investigations of non-critical minor-axis flexural components. The experimental and FEA results were compared to results from a DSM-based design approach. The authors also presented a modification factor for the DSM-based design approach.

Beside effects of initial imperfections and residual stress on cold-formed members were analysed in the publications [4-11]. Load-carrying capacity and material strength at corner also are significant differences in design of hot-rolled and cold-formed members. Yu (2000) indicated that load-carrying capacity of cold formed steel members are limited by buckling stress that are usually less than yield stress of the steel material [12]. Unlike hot-rolled

members, material strength in corners of cold-formed steel members significantly increase by manufacturing process. Ma et al. (2015) specified that 0.2% proof stresses in the corner part with 90° bends increased by up to 34% with effect of cold forming [13].

This paper describes experimental and numerical investigations of the resistance of cold-formed high strength steel angles for polygonal cross sections with different side number in application for wind turbine tubular towers. Thirty-six specimens with different cold-formed angles (90°, 100°, 120°, 140°, 160°, and 170°) and different thicknesses (4 mm and 6 mm) were studied. The initial geometric imperfections of the specimens were determined using the 3D laser scanning method. The magnitudes of initial geometric imperfections for torsional and torsional-flexural buckling and flexural buckling analyses were proposed. The commercial finite element analysis (FEA) programme ABAQUS [14] with shell elements S4R were used for finite element analyses. The influence of yield strength on the FEA was considered with different proof stresses (0.2%, 0.01%, and 0.006%). The experimental results were compared to FEA results. Furthermore, influence of cold-formed angle on non-dimensional slenderness ($\bar{\lambda}$) and reduction factor (χ) curves of the 4 mm thick columns with 90° and 120° cold-formed angles was analysed.

2. Experimental investigation

2.1. Test specimens

In order to investigate the influence of cold-formed angles on the angle resistance, an experimental programme was carried out. Thirty-six angle columns with different thicknesses (4 mm and 6 mm) were studied. The columns were divided into six categories with different cold-formed angles P1 (90°), P2 (100°), P3 (120°), P4 (140°), P5 (160°) and P6 (170°). The width of equal-leg angle (h) of the specimens was 60 mm. Compression tests were carried out on the thirty-six specimens. Figures 1 and 2 show the typical angle specimens with different cold-formed angles.

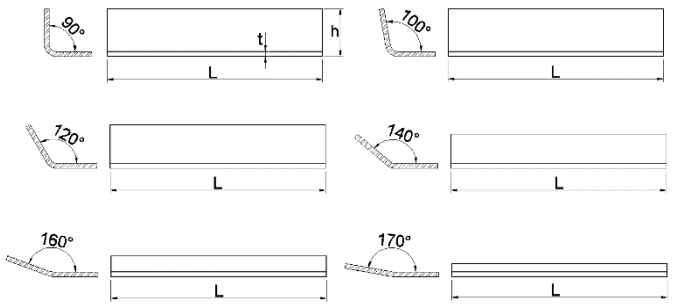

Fig. 1 Typical angle specimens with different cold-formed angles

Fig. 2 4 mm thick specimens with different cold-formed angles

The thicknesses and lengths of the specimens were measured with digital callipers. Each dimension was measured three times. The average values of the measured dimensions and the areas of the cross sections for the specimens are given in Tables 1 and 2. The specimens are labelled as follows: Angle {P1; P2; P3; P4; P5; P6} - Thickness {4 mm; 6 mm} - Test number in the test series {S1; S2; S3}.

Table 1
Average measured dimensions of the 4 mm thick specimens

Specimen	Angle	Thickness (mm)	Length (mm)	Area (mm²)
P1-4-S1	90°	3.96	593	446
P1-4-S2	90°	4.02	594	453
P1-4-S3	90°	4.02	593	453
P2-4-S1	100°	3.97	590	454
P2-4-S2	100°	4.01	593	459
P2-4-S3	100°	3.94	593	451
P3-4-S1	120°	4.04	591	472
P3-4-S2	120°	4.03	590	471
P3-4-S3	120°	4.02	591	470
P4-4-S1	140°	3.98	593	471
P4-4-S2	140°	4.01	592	475
P4-4-S3	140°	4.02	589	476
P5-4-S1	160°	3.95	591	471
P5-4-S2	160°	4.02	593	479
P5-4-S3	160°	4.04	594	482
P6-4-S1	170°	4.04	592	483
P6-4-S2	170°	3.98	590	476
P6-4-S3	170°	3.96	591	474

Table 2
Average measured dimensions of the 6 mm thick specimens

Specimen	Angle	Thickness (mm)	Length (mm)	Area (mm²)
P1-6-S1	90°	6.01	591	654
P1-6-S2	90°	6.03	593	656
P1-6-S3	90°	6.01	594	654
P2-6-S1	100°	5.96	589	665
P2-6-S2	100°	6.01	591	671
P2-6-S3	100°	6.01	592	671
P3-6-S1	120°	6.03	591	695
P3-6-S2	120°	5.92	590	682
P3-6-S3	120°	5.96	590	687
P4-6-S1	140°	6.00	591	704
P4-6-S2	140°	5.96	589	700
P4-6-S3	140°	5.92	593	695
P5-6-S1	160°	6.01	590	715
P5-6-S2	160°	5.95	592	708
P5-6-S3	160°	5.93	594	706
P6-6-S1	170°	6.05	590	723
P6-6-S2	170°	6.03	590	721
P6-6-S3	170°	5.94	591	710

2.2. Test set-up and instruments

A Dartec compression machine with a capacity of 600 kN was used for the compression tests. Fig. 3 shows a typical set-up for the compression tests. Two steel blocks were attached to the compression machine in order to create flat surfaces. The load was applied at the top of the specimen. Displacement control was used for the compression tests. Boundary conditions of the specimens were considered as a clamped support (all translations and rotations were restrained) at the bottom and at the top (all degrees of freedom were fixed except the displacement in the direction of the applied load).

Fig. 3 Set-up for the compression tests

Four LVDTs (linear variable displacement transducers) were used to measure the displacement. Three LVDTs were attached to the machine to measure displacement between the two steel blocks, with the other directly attached to the specimen, see Fig. 4.

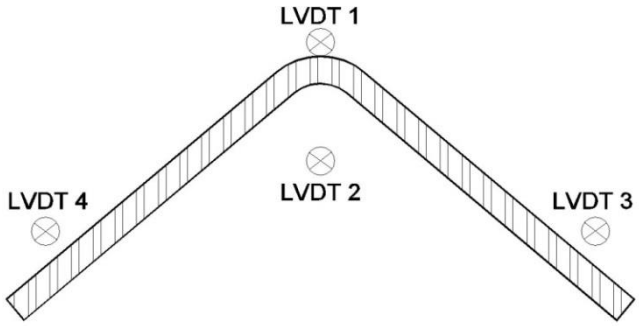

Fig. 4 Positions of LVDTs

2.3. Experimental results

Tables 3 and 4 present the ultimate loads and end shortenings of the 4 mm and 6 mm thick specimens, respectively. The cold-formed angle significantly affected both ultimate loads and end shortenings of the specimens. The average ultimate loads of the 4 mm and 6 mm thick specimens with 90° cold-formed angles were 194 kN and 445 kN, respectively. However, the average ultimate loads of the 4 mm and 6 mm thick specimens with 170° cold-formed angles were just 31 kN and 72 kN, respectively. The average ultimate loads of the 4 mm and 6 mm thick specimens decreased by approximately 84%. The end shortening values also decreased with increasing cold-formed angles from 90° to 170°. The average end-shortenings of the 4 mm and 6 mm thick specimens reduced by 87% and 85%, respectively. The average end shortenings of the 4 mm and 6 mm thick specimens with a cold-formed angle of 170° were 0.25 mm and 0.35 mm, respectively.

Table 3
Ultimate loads and end shortenings of the 4 mm thick specimens

Specimen	Angle	Length (mm)	Area (mm²)	Ultimate load (kN)	End shortening (mm)
P1-4-S1	90°	593	446	195	2.06
P1-4-S2	90°	594	453	191	1.87
P1-4-S3	90°	593	453	195	2.03
P2-4-S1	100°	590	454	195	1.94
P2-4-S2	100°	593	459	199	1.93
P2-4-S3	100°	593	451	207	1.96
P3-4-S1	120°	591	472	203	1.85
P3-4-S2	120°	590	471	200	1.80
P3-4-S3	120°	591	470	198	1.72
P4-4-S1	140°	593	471	194	1.32
P4-4-S2	140°	592	475	194	1.42
P4-4-S3	140°	589	476	187	1.25
P5-4-S1	160°	591	471	81	0.58
P5-4-S2	160°	593	479	80	0.59
P5-4-S3	160°	594	482	79	0.58
P6-4-S1	170°	592	483	28	0.24
P6-4-S2	170°	590	476	33	0.26
P6-4-S3	170°	591	474	31	0.26

Table 4
Ultimate loads and end shortenings of the 6 mm thick specimens

Specimen	Angle	Length (mm)	Area (mm²)	Ultimate load (kN)	End shortening (mm)
P1-6-S1	90°	591	654	443	2.35
P1-6-S2	90°	593	656	446	2.43
P1-6-S3	90°	594	654	445	2.37
P2-6-S1	100°	589	665	446	2.22
P2-6-S2	100°	591	671	466	2.41
P2-6-S3	100°	592	671	451	2.35
P3-6-S1	120°	591	695	450	2.02
P3-6-S2	120°	590	682	440	1.95
P3-6-S3	120°	590	687	442	2.02
P4-6-S1	140°	591	704	369	1.73
P4-6-S2	140°	589	700	389	1.85
P4-6-S3	140°	593	695	339	1.65
P5-6-S1	160°	590	715	147	0.78
P5-6-S2	160°	592	708	141	0.72
P5-6-S3	160°	594	706	147	0.77
P6-6-S1	170°	590	723	70	0.33
P6-6-S2	170°	590	721	73	0.33
P6-6-S3	170°	591	710	72	0.38

Fig. 5 shows the typical deformations of the specimens with cold-formed angles 90°, 120°, and 170° during the tests. Fig. 6 gives typical failure modes of the 4 mm specimens with different cold-formed angles 90°, 100°, 120°, 140°, 160°, and 170°. Cold-formed angles significantly affected buckling behaviour of the specimens. Flexural-torsional buckling occurred in the specimens with cold-formed angles of 90°, 100°, 120°, and 140°. Flexural buckling occurred in the specimens with cold-formed angles of 160° and 170°.

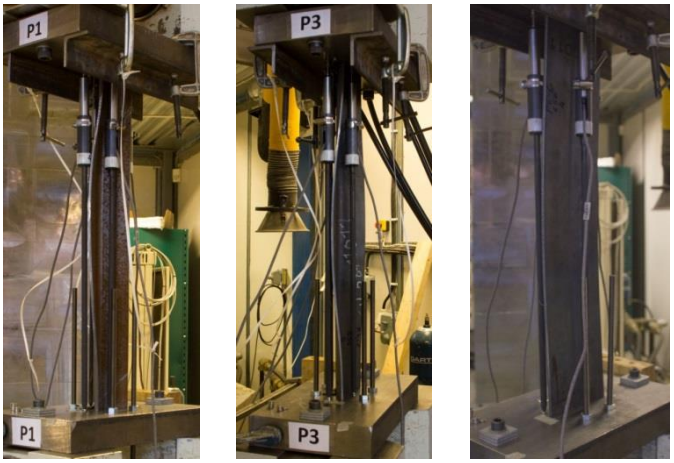

Fig. 5 Typical deformations of the specimens P1 (90°), P3 (120°) and P6 (170°)

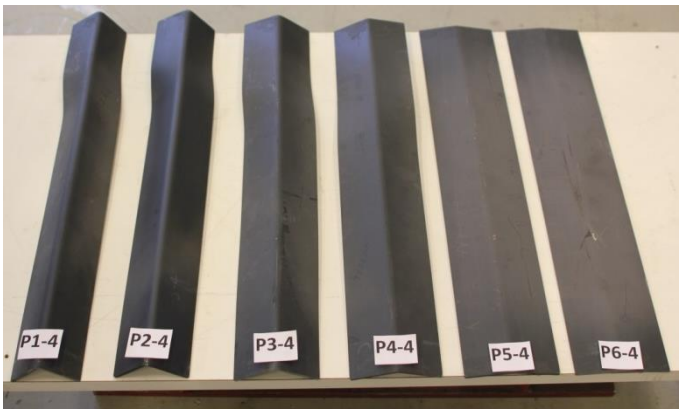

Fig. 6 Typical failure modes of the 4 mm thick specimens P1 (90°), P2 (100°), P3 (120°), P4 (140°) P5 (160°) and P6 (170°)

3. Numerical investigation

3.1. Numerical model

The commercial finite element analysis (FEA) programme ABAQUS [14] was used to simulate the columns with different cold-formed angles under axial compression load. It should be emphasised that the thicknesses of the 4 mm and 6 mm specimens are approximately 0.67% and 1% of their lengths, respectively. In ABAQUS, there are several types of shell elements available [15]. Shell elements S4R (shell elements with four nodes, quadrilateral, reduced numerical integration and a large-strain formulation) were used in this study. Fig. 7 shows a typical FE mesh used for the numerical models. The sizes of shell elements on each side of the columns were approximately 2 mm. The curves at the corner parts were seeded with 8 elements.

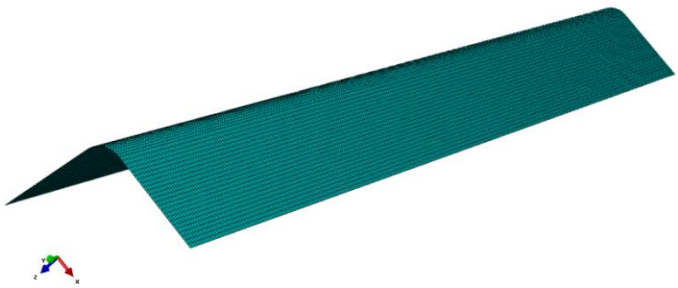

Fig. 7 Typical mesh of the numerical models

Fig. 8 shows the typical boundary conditions used for the numerical models. Numerical models with pined and fixed supports were performed and compared with test results. FEA results from the numerical model with fixed support had good match with test results in terms of load-displacement curve, ultimate load and failure mode. Therefore, numerical models with fixed support were used in this study. A clamped support (all translations and rotations were restrained) was applied at the bottom and at the top, and all degrees of freedom were fixed except the displacement in the direction of the applied load.

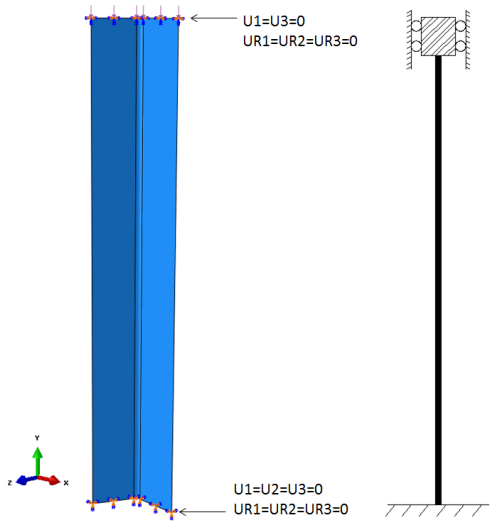

Fig. 8 Typical boundary conditions used for the numerical models

In EN 1993-1-3 [3], influence of cold forming is considered with assumption of increasing yield stress of whole cross sections (corner part and flat part as well) by an average yield stress. In this study, the cold-formed angle specimens were produced by press braking method. In this method, plastic deformation appears in corners of the specimens. It leads to increasing material strength in comparison with original material. An experimental programme using tensile coupon tests was carried out to investigate the mechanical properties of the high strength steel material S650 at the corner and flat parts. In this study, material strengths in corner part and flat part are considered separately.

Key parameters such as yield stress (σ_y), tensile stress (σ_u), and yield strain (ε_y) and tensile strain (ε_u) of the material at the corner and flat parts are shown in Tables 5, 6 and 7. The following nomenclature was adopted for the specimens: Angle of coupon specimen {C1(90°), C2(100°), C3(120°), C4(140°), C5(160°) and F(flat)} - Thickness {4 mm and 6 mm}-Test number in the test series {S1; S2; S3}. In some cases, the failure sections occurred outside the gauge lengths and, hence, those values (C5-4, C4-6, C1-4-S2, C4-4-S1 and C5-6-S1) were not recorded.

Table 5
Key material properties determined from tensile tests of flat coupon specimens

Specimen	Angle	σ_y (N/mm²)	ε_y (%)	σ_u (N/mm²)	ε_u (%)
F-4-S1	180°	762	0.60	802	10.6
F-4-S2	180°	763	0.60	807	8.6
F-4-S3	180°	762	0.60	806	8.5
F-6-S1	180°	801	0.40	845	5.7
F-6-S2	180°	793	0.40	843	6.0
F-6-S3	180°	791	0.40	843	5.9

Table 6
Key material properties determined from tensile tests of 4 mm thick coupon specimens

Specimen	Angle	σ_y (N/mm²)	ε_y (%)	σ_u (N/mm²)	ε_u (%)
C1-4-S1	90°	889	0.62	929	1.18
C1-4-S2	90°	-	-	-	-
C1-4-S3	90°	925	0.64	951	1.24
C2-4-S1	100°	932	0.64	948	1.02
C2-4-S2	100°	927	0.64	948	1.12
C2-4-S3	100°	914	0.64	944	1.16
C3-4-S1	120°	837	0.60	895	1.25
C3-4-S2	120°	865	0.61	917	1.17
C3-4-S3	120°	859	0.61	898	1.15
C4-4-S1	140°	-	-	-	-
C4-4-S2	140°	839	0.60	876	1.51
C4-4-S3	140°	831	0.60	859	1.07

Table 7
Key material properties determined from tensile tests of 6 mm thick coupon specimens

Specimen	Angle	σ_y (N/mm²)	ε_y (%)	σ_u (N/mm²)	ε_u (%)
C1-6-S1	90°	782	0.57	896	1.50
C1-6-S2	90°	830	0.60	923	1.46
C1-6-S3	90°	874	0.62	896	1.22
C2-6-S1	100°	843	0.60	898	1.37
C2-6-S2	100°	861	0.61	893	1.31
C2-6-S3	100°	853	0.61	890	1.37
C3-6-S1	120°	878	0.62	916	1.33
C3-6-S2	120°	883	0.62	917	1.32
C3-6-S3	120°	845	0.60	905	1.69
C5-6-S1	160°	-	-	-	-
C5-6-S2	160°	778	0.57	867	1.67
C5-6-S3	160°	826	0.59	881	1.34

Multi-linear constitutive model was used to model the material properties, Fig. 9. In the commercial finite element analysis (FEA) programme ABAQUS, the engineering stress-strain relationships need to be converted into the form of true stress and true plastic strains using Eq. (1) and (2) [15]:

$$\sigma_{true} = \sigma_{eng}(1+\varepsilon_{eng}) \quad (1)$$

$$\varepsilon_{true,p} = \ln(1+\varepsilon_{eng}) - \frac{\sigma_{true}}{E} \quad (2)$$

where: σ_{true} is true stress, σ_{eng} is engineering stress, $\varepsilon_{true,p}$ is true plastic strain, and ε_{eng} is engineering strain.

Residual stress in cold-formed steel plain angle columns was studied by E. Ellobody and B. Young [6]. The authors specified that ultimate load and shortening of the columns with and without residual stress are almost identical. Therefore, residual stress was not considered in this study.

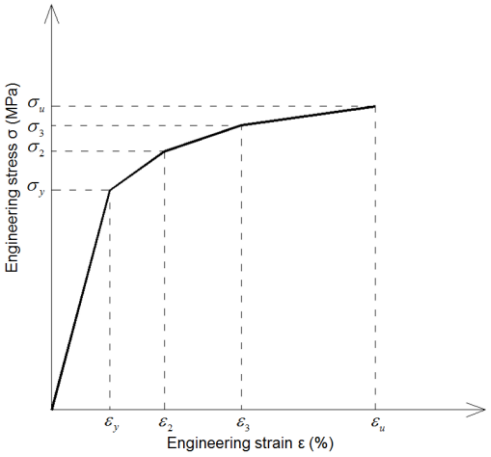

Fig. 9 Material model

3.2. Initial geometric imperfections

Initial geometric imperfections significantly affect the resistance of the specimens. Therefore, the geometric imperfections of the specimens were determined before testing. There are several methods to determine initial geometric imperfections of specimens. B. W. Schafer et al. [16] used a milling machine, a direct current differential transformer (DCDT) and a computer to measure the initial geometric imperfections of eleven specimens. This method was also used to determine the geometric imperfections of S460NH and S690QH specimens by J. Wang et al. [17]. A theodolite with micrometer plates was used to measure the geometric imperfections at the tips of the legs and at the corners of thirty cold-formed angles [4]. B. Young used two theodolites to obtain the geometric imperfections at the mid-length and near both ends of nineteen cold-formed steel plain angle columns [5]. E. Ellobody and B. Young used a coordinate measuring machine to measure the geometric imperfections at the middle and quarter length of their specimens [6]. Tran et al. used a 3D laser scanning method to measure the geometric imperfections of thirty-two cold-formed circular and polygonal specimens with and without openings [18]. In this study, the 3D laser scanning method was also used to measure the initial geometric imperfections of the thirty-six cold-formed angles. Fig. 10 shows the initial geometric imperfections of the P4-4-S2 specimen.

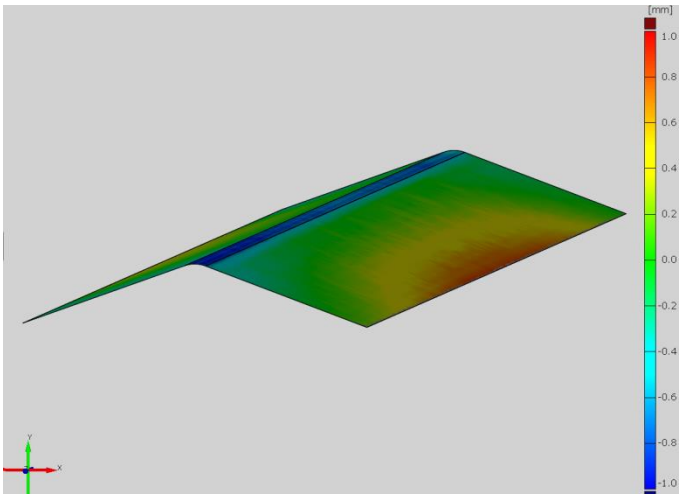

Fig. 10 Initial geometric imperfections of the P4-4-S2 specimen

In order to determine geometric imperfections of the specimens, approximately 4100 points on the surface of each specimen were considered. The biggest geometric imperfection amplitudes of the specimens at the sides (e_t) and at the middle (e_l) of angles are given in Tables 8 and 9. Direction of e_t and e_l are perpendicular to side surface and vertical direction of specimen respectively.

Table 8
Initial geometric imperfections of the 4 mm thick specimens

Specimen	Angle	Thickness (mm)	Length (mm)	Max imperfection amplitude e_t (mm)	e_l (mm)
P1-4-S1	90°	3.96	593	0.76	0.64
P1-4-S2	90°	4.02	594	0.90	0.61
P1-4-S3	90°	4.02	593	0.60	0.50
P2-4-S1	100°	3.97	590	0.67	0.58
P2-4-S2	100°	4.01	593	0.93	0.70
P2-4-S3	100°	3.94	593	0.96	0.76
P3-4-S1	120°	4.04	591	0.60	0.53
P3-4-S2	120°	4.03	590	0.71	0.71
P3-4-S3	120°	4.02	591	0.70	0.63
P4-4-S1	140°	3.98	593	0.80	0.80
P4-4-S2	140°	4.01	592	0.72	0.72
P4-4-S3	140°	4.02	589	0.71	0.69
P5-4-S1	160°	3.95	591	0.80	0.79
P5-4-S2	160°	4.02	593	0.81	0.78
P5-4-S3	160°	4.04	594	0.90	0.88
P6-4-S1	170°	4.04	592	0.70	0.67
P6-4-S2	170°	3.98	590	0.59	0.51
P6-4-S3	170°	3.96	591	0.74	0.65
Mean				0.76	0.67
Standard deviation				0.11	0.11

Table 9
Initial geometric imperfections of the 6 mm thick specimens

Specimen	Angle	Thickness (mm)	Length (mm)	Max imperfection amplitude e_t (mm)	e_l (mm)
P1-6-S1	90°	6.01	591	1.04	0.94
P1-6-S2	90°	6.03	593	1.11	0.80
P1-6-S3	90°	6.01	594	1.04	0.72
P2-6-S1	100°	5.96	589	1.17	0.83
P2-6-S2	100°	6.01	591	1.25	0.82
P2-6-S3	100°	6.01	592	0.62	0.87
P3-6-S1	120°	6.03	591	0.90	0.69
P3-6-S2	120°	5.92	590	1.01	0.65
P3-6-S3	120°	5.96	590	0.89	0.62
P4-6-S1	140°	6.00	591	0.75	0.73
P4-6-S2	140°	5.96	589	0.94	0.71
P4-6-S3	140°	5.92	593	0.70	0.82
P5-6-S1	160°	6.01	590	0.61	0.74
P5-6-S2	160°	5.95	592	0.78	0.84
P5-6-S3	160°	5.93	594	0.71	0.51
P6-6-S1	170°	6.05	590	0.72	0.65
P6-6-S2	170°	6.03	590	1.14	0.60
P6-6-S3	170°	5.94	591	1.04	0.91
Mean				0.91	0.75
Standard deviation				0.20	0.12

According to EN 1993-1-5 [19], in relation to local buckling of a panel or subpanel with a short span a or b, the magnitude of the equivalent geometric imperfections is the lower value of a/200 and b/200. In respect of flexural buckling, according to EN 1993-1-1 [20], the magnitudes of initial imperfections for elastic analysis and plastic analysis are L/200 and L/150 respectively (buckling curve c). The magnitudes of initial geometric imperfections have been described in several papers. The average geometric imperfections of 30 cold-formed angles at the tips of the legs and at the corners were L/1305 and L/2310, respectively [4]. The authors also specified that the geometric imperfections at the tips were much higher than at the corners. F. Yang et al. used L/750 at the middle of cold-formed angles for the initial overall geometric imperfection [7]. E. Mesacasa Jr et al. used geometric imperfection amplitude L/1000 at middle height of thin-walled equal-leg angle columns in FEA for flexural-torsional buckling and flexural buckling analyses [27]. According to EN 1090-2:2008+A1:2011, the permitted deviation Δ of cold-formed profiled sheets should be $\Delta \leq \pm b/50$ (b is the nominal width) [25]. It should be emphasised that the width of the equal-leg angle (h) of the specimens was 60 mm. Therefore, the maximum imperfection amplitudes of our specimens were within the recommendation according to EN 1090-2:2008+A1:2011.

In attempt to determine geometric imperfections for cold-formed angle specimens, collected data on geometric imperfections of thirty-six specimens were performed. Fig. 11 shows the ratios between the maximum geometric imperfection magnitude at the sides of the angles and the thicknesses of the specimens, as a percentage. Fig. 12 shows the ratios between the lengths and the maximum geometric imperfection magnitude at the middle of the specimens. Average values of the ratios are determined and also presented in Figs 11 and 12. The magnitude of initial geometric imperfections for local and torsional/torsional-flexural buckling and flexural buckling analyses of cold-formed angle specimens are proposed as 17% t and L/855 respectively, where L and t are the length and thickness of the specimen, respectively. It emphasized that the specimens in this study were provided by Ruukki Company in Finland.

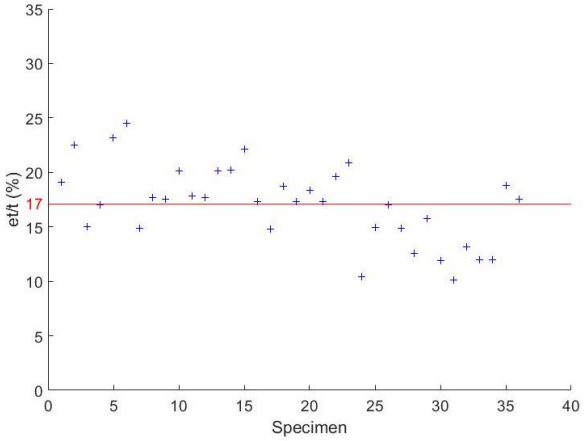

Fig. 11 Ratio of percentage between maximum initial geometric imperfection at sides and thickness of each specimen

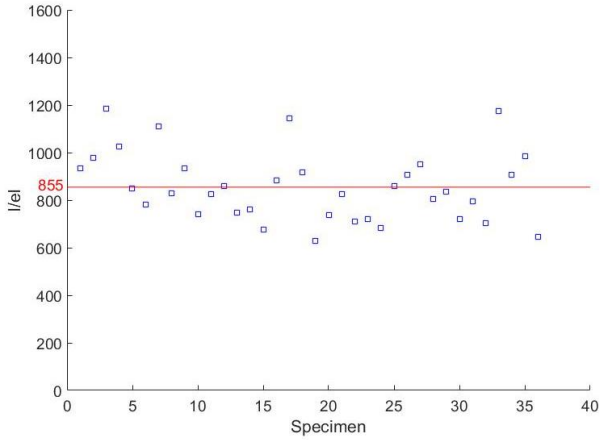

Fig. 12 Ratio between maximum initial geometric imperfection at the middle and length of each specimen

3.3. Influence of yield strength on the FEA

Proof stress significantly affects the resistance of finite element analysis (FEA) models [21]. According to EN 1993-1-6, if the behaviour between stress and strain is nonlinear, the yield strength should be taken as 0.2% proof stress [22]. However, N.S. Ottosen and M. Ristinmaa specified that offset strains used in most scientific experimental investigations are much smaller than 0.2% [23].

D. Rees recommended that offset strains are in the range from 0.001% to 0.01% [24]. In this study, 0.2%, 0.01% and 0.006% proof stresses were used to investigate the influence of proof stress on the resistance of the FEA models. The specimens studied had different thicknesses (4 mm and 6 mm) and different cold-formed angles (90°, 100°, 120°, and 140°). Resistance values from the FEA were compared to corresponding results from the experiments, see Table 10. Mean values and standard deviation values are also shown in this table. Mean values of resistance ratios between experimental and FEA results with 0.2%, 0.01%, and 0.006% proof stresses were 0.91, 0.99, and 1.06, respectively. The difference in average between the experimental and FEA results with 0.01% proof stress was just 1%. Therefore, 0.01% proof stress was used in this study.

Table 10
Initial geometric imperfections of the 6 mm thick specimens

Specimen	Angle	Ultimate load (kN)						
		Experiment	FEA					
		Ptest	P0.2	P0.01	P0.006	Ptest/P0.2	Ptest/P0.01	Ptest/P0.006
P1-4-S1	90°	195	211	196	191	0.93	1.00	1.02
P1-6-S3	90°	445	489	423	375	0.91	1.05	1.19
P2-4-S2	100°	199	214	200	194	0.93	0.99	1.02
P2-6-S1	100°	446	498	448	411	0.89	0.99	1.08
P3-4-S2	120°	200	217	201	194	0.92	1.00	1.03
P3-6-S1	120°	450	522	467	426	0.86	0.96	1.06
P4-4-S2	140°	194	213	203	196	0.91	0.96	0.99
Mean						0.91	0.99	1.06
Standard deviation						0.02	0.03	0.06

3.4. Finite element model validation

Resistance comparisons of the specimens with different thicknesses and different cold-formed angles between the experimental and FEA results are presented in Table 10. It should be noted that materials of corner part and flat part in the numerical models were modelled separately based on tensile coupon tests. Therefore, FEA results of some cold-formed angles are not presented in Table 11 because of lacking data from the tensile coupon tests. The mean and standard deviation values were 1.01 and 0.04, respectively. The difference in average between the experimental and FEA results was just 1%. The good agreement between ultimate loads derived from the FEA and experimental results validate the simulations. It should be noticed that different materials were used for the different parts (flat and corner parts) and the initial geometric imperfections of the specimens were determined using the 3D laser scanning method described in section 3.2. Experimental and numerical load-displacement curves for the 4 mm thick specimen with 90° cold-formed angle and 120° cold-formed angle are presented in Figs 13 and 14 respectively. They show good agreement in terms of shapes and ultimate loads. Figs 15 and 16 show the deformation and failure mode of the 4 mm thick specimen with 100° cold-formed angle, respectively. The experimental results matched those from the FEA well.

Table 11
Comparisons between experimental and FEA results

Specimen	Angle	Thickness	Length	Ultimate load (kN)		
		(mm)	(mm)	FEA (PFEA)	Experiment (Ptest)	PFEA/Ptest
P1-4-S1	90°	3.96	593	196	195	1.00
P1-4-S2	90°	4.02	594	197	191	1.03
P1-4-S3	90°	4.02	593	197	195	1.01
P2-4-S1	100°	3.97	590	200	195	1.03
P2-4-S2	100°	4.01	593	200	199	1.01
P2-4-S3	100°	3.94	593	200	207	0.97
P3-4-S1	120°	4.04	591	200	203	0.99
P3-4-S2	120°	4.03	590	201	200	1.01
P3-4-S3	120°	4.02	591	201	198	1.01
P4-4-S1	140°	3.98	593	202	194	1.04
P4-4-S2	140°	4.01	592	203	194	1.04
P4-4-S3	140°	4.02	589	203	187	1.08
P1-6-S1	90°	6.01	591	423	443	0.95
P1-6-S2	90°	6.03	593	421	446	0.94
P1-6-S3	90°	6.01	594	423	445	0.95
P2-6-S1	100°	5.96	589	448	446	1.01
P2-6-S2	100°	6.01	591	445	466	0.96
P2-6-S3	100°	6.01	592	462	451	1.02
P3-6-S1	120°	6.03	591	467	450	1.04
P3-6-S2	120°	5.92	590	463	440	1.05

P3-6-S3	120°	5.96	590	467	442	1.06
Mean						1.01
Standard deviation						0.04

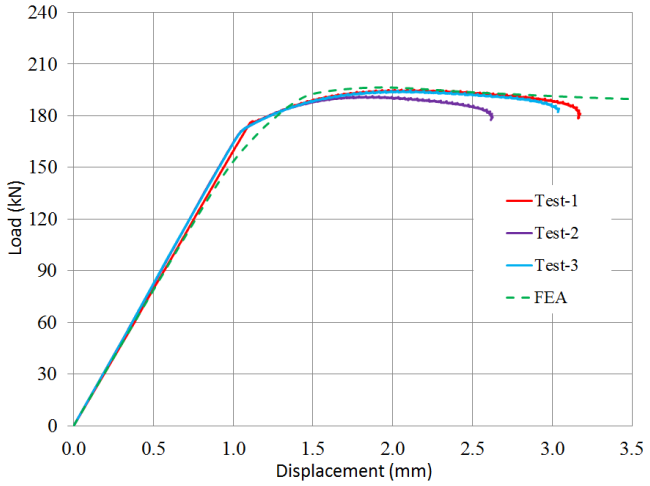

Fig. 13 Load-displacement curves obtained from the FEA and test results for 4 mm thick specimens with 90° cold-formed angle

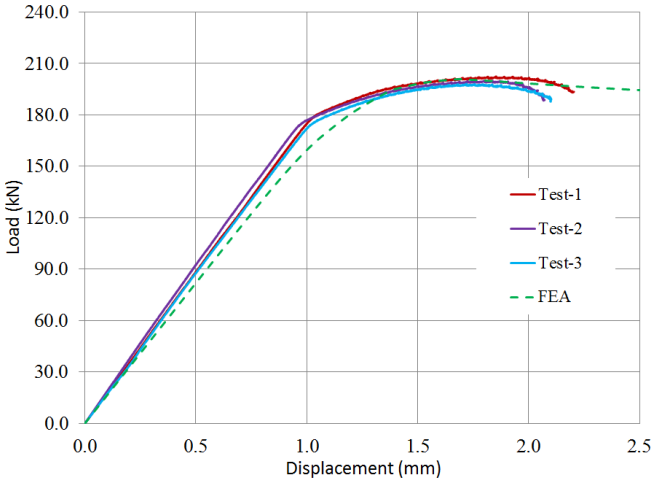

Fig. 14 Load-displacement curves obtained from the FEA and test results for 4 mm thick specimens with 120° cold-formed angle

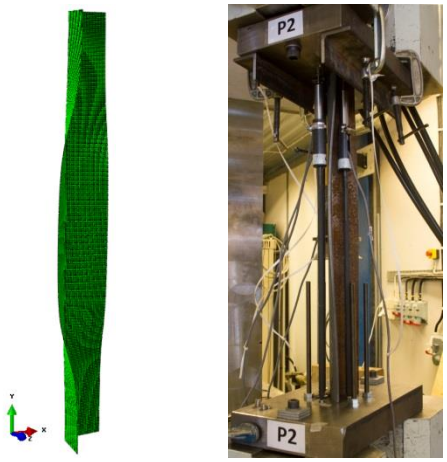

Fig. 15 Deformation of the 4 mm thick specimen with 100° cold-formed angle (FEA and experimental results)

Fig. 16 Failure mode of the 4 mm thick specimen with 100° cold-formed angle (experimental and FEA results)

4. Parametric study

Behaviour of angle columns with various lengths were numerically investigated and presented in [26-27]. Dinis et al [26] and Mesacasa Jr. et al [27] used the commercial finite element analysis (FEA) programmes ABAQUS and ANSYS with shell elements for their studies respectively. Dinis et al [26] used cross section L70x70x1.2 mm3 and Mesacasa Jr. et al [27] used cross section L70x70x2.0 mm3 for the columns. It is worth to mention that class of the cross-sections is 4.

The authors specified that behaviours of short-to-intermediate and intermediate-to-long columns are flexural-torsional buckling and pure flexural buckling, respectively and 'transition length' between the two buckling behaviours. In the transition length, behaviour of the columns is coupling between two global buckling (flexural-torsional buckling and pure flexural buckling). Ultimate strengths of the columns significantly grow as the length reaches the transition value [27]. It notes that transition value is the coincident flexural-torsional and flexural critical buckling load.

In this work, the commercial finite element analysis (FEA) programmes ABAQUS [14] used to determine critical loads of the column with various lengths. Fig. 17 shows relationship between critical loads and column lengths of the cross section L60x60x4 mm3. The curve presented by Mesacasa Jr. et al in [27] is also showed in this figure. It notes that F and P in the curve from Mesacasa Jr. et al are fixed and pined boundary conditions respectively. The curves of the L70x70x2 mm3 columns and L60x60x4 mm3 columns with 90° cold-formed angle show good match in term of shape and trend.

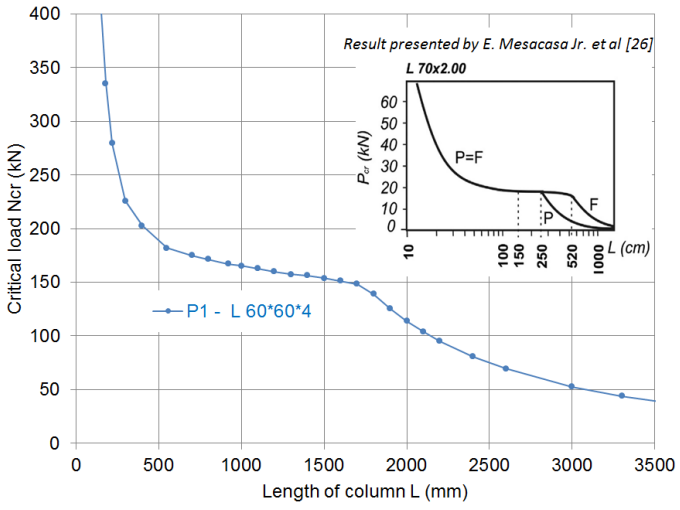

Fig. 17 Critical load and column length curve of the 4 mm thick column with 90° cold-formed angle

After FE models validated in section 3.4, a series of FE models were developed to investigate relationships between non-dimensional slenderness ($\bar{\lambda}$) and reduction factor (χ) curves of the columns with 90° and 120° cold-formed angles. Cross-section dimensions of the columns were fixed with 4 mm thickness and 60 mm width of equal-leg angle. Slenderness of the columns was determined by changing length of the columns. Material in corner part and flat part of the columns were modelled separately based on tensile coupon tests. Initial geometric imperfections of the columns were used as 17% of thickness and 1/855 of length of the columns for torsional-flexural buckling behaviour and flexural buckling behaviour respectively. Boundary

conditions of the columns were a clamped support (all translations and rotations were restrained) at the bottom and at the top (all degrees of freedom fixed except the displacement in the direction of the applied load).
The reduction factor was calculated as follows:

$$\chi = \frac{N_{ult}}{N_y} \tag{3}$$

where N_{ult} is the ultimate load determined by experiment or from FEA, and N_y is determined using the following equation:

$$N_y = A_{corner} f_{y,corner} + A_{eff} f_{y,flat} \tag{4}$$

where A_{corner}, A_{eff} are the areas of the corner part and the effective area of the flat part, respectively, $f_{y,corner}$ and $f_{y,flat}$ are the yield strengths of the corner part and the flat part, respectively. It should be noted that the class of the specimens is 4. According to EN 1993-1-5 [19], a gross cross-sectional area for a class 4 cross section is reduced to an effective area of a compression zone. The effective area is determined by Eq. (5).

$$A_{eff} = \rho A_g \tag{5}$$

where ρ is the reduction factor for plate buckling, and A_g is the gross cross-sectional area. The reduction factor for the plate buckling is determined as follows:

$$\rho = 1 \quad \text{for} \quad \bar{\lambda}_\rho \le 0.748 \tag{6}$$

$$\rho = \frac{\bar{\lambda}_\rho - 0.188}{\bar{\lambda}_\rho^2} \le 1.0 \quad \text{for} \quad \bar{\lambda}_\rho > 0.748 \tag{7}$$

where: $$\bar{\lambda}_p = \frac{h/t}{28.4\varepsilon\sqrt{k_\sigma}} \tag{8}$$

and h is the width of the equal-leg angle, t is the thickness, k_σ is the buckling factor, and

$$\varepsilon = \sqrt{\frac{235}{f_{y,flat}}} \tag{9}$$

The non-dimensional slenderness $\bar{\lambda}$ is obtained from the following equation:

$$\bar{\lambda} = \sqrt{\frac{A_{corner} f_{y,corner} + A_{eff} f_{y,flat}}{N_{cr}}} \tag{10}$$

where N_{cr} is the elastic critical force for flexural buckling and torsional-flexural buckling.

Fig. 18 presented relationship between the non-dimensional slenderness and reduction factor curves of the 4 mm thick columns with 90° and 120° cold-formed angles. The figure also shows results tested by Popovic et al [4] and test results of the P1 and P3 columns with approximately 600 mm length. Popovic et al [4] tested columns with L50x50x2.5 mm3 cross-section under compression. The material properties in corner and flat part and compression test results of the L50x50x2.5 mm3 columns presented in Tables 12 and 13 respectively. The test results agree well to the FEA results.

Table 12
Tensile coupon test results from Popovic et al [4]

Section	Material	$f_{y\ static}$ (MPa)	$f_{y\ static}$ (MPa)	E (MPa)	e_u (%)
L50x50x2.5	Corner	568	618	200516	10
L50x50x2.5	Flat	396	475	208318	23

Table 13
Compression test results* from Popovic et al [4]

Section*	Sample length L (mm)*	Ultimate load N_{test} (kN)*	Reduction factor $\frac{N_{test}}{N_y}$
L50x50x2.5	550	54.0	0.85
L50x50x2.5	970	41.5	0.65
L50x50x2.5	1379	37.0	0.58
L50x50x2.5	1747	31.3	0.49
L50x50x2.5	2199	26.4	0.41
L50x50x2.5	2598	22.3	0.35

Characteristic comparison between the 120° and 90° cross-sections is presented in Table 14. The torsion constant, warping constant and second moment of area for major axis of the 120° cross-section are 4%, 12% and 57% higher than 90° cross-section respectively. It is worth to note that, in this work, slenderness of the columns was determined by changing length of the columns. The column length decrease (non-dimensional slenderness decrease) causes increasing effect of cross section characteristic (for the major axis) on the flexural-torsional buckling. It leads the reduction factor of 120° cross-section column is higher than 90° cross-section column as the non-dimensional slenderness decreases.

Table 14
Characteristic comparison between 90° and 120° cross-sections

Characteristic of cross section	Cross section P3 (120°)	Cross section P1 (90°)	$\frac{P_3}{P_1}$
Torsion constant (I_t mm^4)	2426	2328	1.04
Warping constant (I_w mm^6)	691070	618780	1.12
Second moment of area for major axis (I_y mm^4)	407680	260350	1.57

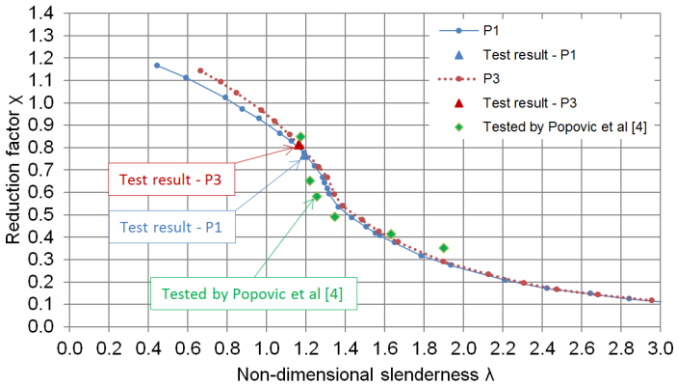

Fig. 18 Non-dimensional slenderness and reduction factor curves of the 4 mm thick columns with 90° and 120° cold-formed angles

5. Conclusions

The resistance of the thirty-six specimens with different thicknesses (4 mm and 6 mm) and different cold-formed angles (90°, 100°, 120°, 140°, 160°, and 170°) was investigated experimentally. Numerical models were developed and calibrated against the experimental results. Based on experimental and FEA results, the following conclusions are suggested:

- The resistance of the specimens significantly decreases by 84% with increasing cold-formed angles from 90° to 170°.
- The initial geometric imperfections of the thirty-six specimens are investigated using the 3D laser scanning method. Magnitudes of the initial geometric imperfection for torsional and torsional-flexural buckling and flexural buckling analyses are proposed 17% b and L/855 respectively.
- The influence of 0.2%, 0.01%, and 0.006% proof stresses on the resistances in FEA are considered. The differences between experimental and FEA results corresponding to 0.2%, 0.01% and 0.006% proof stresses are 9%, 1%, and 6% respectively.
- Relationships between non-dimensional slenderness ($\bar{\lambda}$) and reduction factor (χ) of the 4 mm thick columns with 90° and 120° cold-formed angles were analysed and presented.

Acknowledgements

The authors wish to thank the Research Fund for Coal and Steel for financially supporting the research in this paper through the Research Project HISTWIN 2 (RFSR-CT-2010-00031).

References

[1] AS/NZS-4600, Cold-formed Steel Structures, Australian/New Zealand standard, 2005.

[2] AISI-S100-12, North American Specification for the Design of Cold Formed Steel Structural Members, AISI, 2012.

[3] EN 1993-1-3, Design of Steel Structures, Part 1-3: General Rules – Supplementary Rules for Cold-formed Members and Sheeting, Brussels, Belgium: European Committee for Standardization, 2006.

[4] Popovic D., Hancock G.J. and Rasmussen K.J.R., "Axial compression tests of cold-formed angles", Journal of Structural Engineering, 125, 515–523, 1999.

[5] Young B., "Tests and design of fixed-ended cold-formed steel plain angle columns", Journal of Structural Engineering, 130, 1931–1940, 2004.

[6] Ellobody E. and Young B., "Behavior of cold-formed steel plain angle columns", Journal of Structural Engineering, 131, 457–466, 2005.

[7] Yang F., Han J., Yang J. and Li Z., "Study on the buckling behaviour of cold-formed angles in transmission towers", International Journal of Steel Structures, 11, 495-508, 2011.

[8] Silvestre N., Dinis P.B. and Camotim D., "Developments on the design of cold-formed steel angles", Journal of Structural Engineering, 139, 680–694, 2013.

[9] Shifferaw Y. and Schafer B.W., "Cold-formed steel lipped and plain angle columns with fixed ends", Thin-walled Structures, 80, 142–152, 2014.

[10] Doležal J. and Podgayskyy M., "Resistance of cold-formed L-columns made of high strength steel", Master thesis, 2014.

[11] Landesmann A., Camotim D., Dinis P.B. and Cruz R., "Short-to-intermediate slender pin-ended cold-formed steel equal-leg angle columns: Experimental investigation, numerical simulations and DSM design", Engineering Structures, 132, 471–493, 2017.

[12] Yu W.W., ''Cold-formed Steel Design'', John Wiley and Sons, 2000.

[13] Ma J.L., Chan T.M. and Young B., "Material properties and residual stresses of cold-formed high strength steel hollow sections", Journal of Constructional Steel Research, 109, 152–165, 2015.

[14] Abaqus 6.12-1, Simulia Dassault Systmes, 2012.

[15] Abaqus/Standard User's Manual, Version 6.12.

[16] Schafer B.W. and Peköz T., "Computational modeling of cold-formed steel: characterizing geometric imperfections and residual stresses", Journal of Constructional Steel Research, 47, 193–210, 1998.

[17] Wang J., Afshan S. and Schillo N., Theofanous, M., Feldmann, M., Gardner, L., "Material properties and compressive local buckling response of high strength steel square and rectangular hollow sections", Engineering Structures, 130, 297–315, 2017.

[18] Tran A.T., Veljkovic M., Rebelo C. and Simões da Silva L., "Resistance of cold-formed high strength steel circular and polygonal sections - Part 1: Experimental investigations", Journal of Constructional Steel Research, 120, 245–257, 2016.

[19] EN 1993-1-5, Design of Steel Structures, Part 1-5: Plated Structural Elements, Brussels, Belgium: European Committee for Standardization, 2006.

[20] EN 1993-1-1, Design of Steel Structures, Part 1-1: General Rules and Rules for Buildings, Brussels, Belgium: European Committee for Standardization, 2005.

[21] Tran A.T., Veljkovic M., Rebelo C. and Simões da Silva, L., "Resistance of cold-formed high strength steel circular and polygonal sections - Part 2: Numerical investigations", Journal of Constructional Steel Research, 125, 227–238, 2016.

[22] EN 1993-1-6, Design of Steel Structures, Part 1-6: Strength and Stability of Shell Structures, Brussels, Belgium: European Committee for Standardization, 2007.

[23] Ottosen N.S. and Ristinmaa M., "The Mechanics of Constitutive Modeling", Elsevier, 2005.

[24] Rees R., "Basic Engineering Plasticity: An Introduction With Engineering and Manufacturing Applications", Elsevier, 2006.

[25] EN 1090-2:2008+A1:2011, Execution of Steel Structures and Aluminium Structures, Part 2: Technical Requirements for Steel Structures, Brussels, Belgium: European Committee for Standardization, 2011.

[26] Dinis P.B., Camotim D. and Silvestre N., "On the mechanics of thin-walled angle column instability", Thin-walled Structures, 52, 80–89, 2012.

[27] Mesacasa E. Jr., Dinis P.B., Camotim D. and Malite M., "Mode interaction in thin-walled equal-leg angle columns", Thin-walled Structures, 81, 138–149, 2014.